

HiLM-D: Towards High-Resolution Understanding in Multimodal Large Language Models for Autonomous Driving

Xinpeng Ding^{1,2}, Jianhua Han², Hang Xu², Wei Zhang², Xiaomeng Li¹,

¹The Hong Kong University of Science and Technology

²Huawei Noah's Ark Lab

Abstract

Autonomous driving systems generally employ separate models for different tasks resulting in intricate designs. For the first time, we leverage singular multimodal large language models (MLLMs) to consolidate multiple autonomous driving tasks from videos, *i.e.*, the Risk Object Localization and Intention and Suggestion Prediction (ROLISP) task. ROLISP uses natural language to simultaneously identify and interpret risk objects, understand ego-vehicle intentions, and provide motion suggestions, eliminating the necessity for task-specific architectures. However, lacking high-resolution (HR) information, existing MLLMs often miss small objects (*e.g.*, traffic cones) and overly focus on salient ones (*e.g.*, large trucks) when applied to ROLISP. We propose HiLM-D (Towards **H**igh-Resolution Understanding in MLLMs for Autonomous Driving), an efficient method to incorporate HR information into MLLMs for the ROLISP task. Especially, HiLM-D integrates two branches: (i) the low-resolution reasoning branch, can be any MLLMs, processes low-resolution videos to caption risk objects and discern ego-vehicle intentions/suggestions; (ii) the high-resolution perception branch (HR-PB), prominent to HiLM-D, ingests HR images to enhance detection by capturing vision-specific HR feature maps and prioritizing all potential risks over merely salient objects. Our HR-PB serves as a plug-and-play module, seamlessly fitting into current MLLMs. Experiments on the ROLISP benchmark reveal HiLM-D's notable advantage over leading MLLMs, with improvements of 4.8% in BLEU-4 for captioning and 17.2% in mIoU for detection.

Introduction

The modern autonomous driving system integrates a range of tasks including perception, prediction and planning (Caesar et al. 2020). Conventional methods often rely on separate models for each task, resulting in a complex and cumbersome process (Ngiam et al. 2021), as shown in Fig. 1 (a). In recent years, there have been efforts to address this issue. For example, UniAD (Hu et al. 2023) proposes a holistic design that integrates multiple driving tasks into an end-to-end framework. Despite this integration, these models still rely on distinct sub-networks for specific tasks, such as TrackFormer for object detection and tracking, MapFormer for

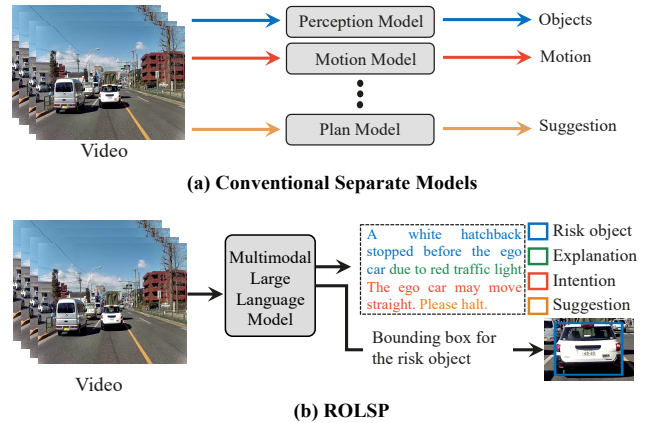


Figure 1: **Comparison of different tasks.** (a) Conventional methods often employ separate models for different tasks. (b) Risk Object Localization and Intention and Suggestion Prediction (ROLISP). Given a video, ROLISP uses a unified multimodal large language model to perform multi-tasks in the caption manner, eliminating the necessity for task-specific architectures.

map segmentation, etc. Contrastingly, human drivers inherently streamline this process, *i.e.*, instantaneously accomplishes perception and decision-making without the need for disparate modules. Recent advancements in multimodal large language models (MLLMs), *e.g.*, MiniGPT-4 (Zhu et al. 2023), LLaVA (Liu et al. 2023), have showcased their proficiency in handling multimodal tasks using natural language paradigms (Liu et al. 2023; Zhu et al. 2023; Dai et al. 2023; Chen et al. 2023; Wang et al. 2023). In autonomous driving, some researchers have proposed using natural captions as a unified output across tasks (Malla et al. 2023; Jin et al. 2023). Inspired by these developments, this paper leverages a singular MLLM to tackle multiple autonomous driving tasks, *i.e.*, Risk Object Localization and Intention and Suggestion Prediction (ROLISP). As shown in Fig. 1 (b), ROLISP directly generates (1) a caption that discriminates the most important traffic objects (*e.g.*, cars, traffic cones and so on), explains why the found object is the risk (if any) and predicts intention and motion suggestion for the ego-car based on the risk object and (2) a bounding box for the found risk object.

However, naively applying current MLLMs to ROLISP would face two problems, *i.e.*, inadequate detection performance for the found risk object and over-attention on large objects leading to misidentification (refer to examples in Fig.2). The reason may come from two aspects. Firstly, due to the data, memory and computation cost limitations, prevalent MLLMs invariably input images with the single small size (*i.e.*, 224×224) for training. However, employing high-resolution (HR) images or feature maps is universally regarded as the preminent and productive strategy to augment the perception in autonomous driving (Sun et al. 2020). Although increasing the resolution of input videos is intuitive, this would incur considerable computation costs, especially for LLMs that require massive computational resources. Second, the vision encoders of current MLLMs are generally the plain vision transformer (ViT) (Dosovitskiy et al. 2020), pre-trained on massive vision-text pairs (Li et al. 2023). Compared with its variants, *e.g.*, Swin Transformer (Liu et al. 2021) and convolution neural networks (CNNs), the plain ViT lacks vision-specific inductive biases (*e.g.*, local connectivity and spatial invariance), leading to slower convergence and lower performance in detection tasks (Chen et al. 2022; Wang et al. 2022).

To address the above problems, we present HiLM-D (Towards High-Resolution Understanding in MLLMs for Autonomous Driving), an efficient framework that leverages the vast knowledge stored in MLLMs, while comprising HR information for ROLISP. The proposed HiLM-D consists of two branches, *i.e.*, a low-resolution reasoning branch (LR-RB) and a high-resolution perception branch (HR-PB). LR-RB, can be any MLLMs, aims to receive the low-resolution (LR) videos as input and generate the caption for the risk object with explanations and ego-vehicle intention/suggestion. HR-PB is the key component of HiLM-D that incorporates the perception ability into the MLLMs to promote ROLISP in a parameter-efficient and computation-friendly way. To achieve this, HR-PB processes the high-resolution image sampled from videos, producing highlighted HR feature maps enriched with vision-specific priors and emphasizing potential high-risk object regions. The enriched features not only benefit the detection of small objects due to the HR but also leverage the vision-specific priors (*e.g.*, local connectivity, spatial invariance) to improve the detection across all objects. By incorporating the highlighted features emphasizing potential high-risk object regions into LR-RB, the LLM can assess and decide which one needs the most attention, thus mitigating the over-attention of large objects. Note that our HiLM-D is a plug-and-play module that can be easily integrated into existing MLLMs.

We conduct experiments on the constructed dataset DRAMA-ROLISP, demonstrating that our proposed method can outperform the current MLLMs by 4.8% on BLEU-4 for captioning and 17.2% on mIoU for detection. The ablation study and visualization illustrate the effectiveness of each proposed module.

The contributions of our paper are summarized as follows:

- We harness MLLMs to address multiple autonomous driving tasks, *i.e.*, ROLISP, through natural language paradigms. To our knowledge, this is the first exploration

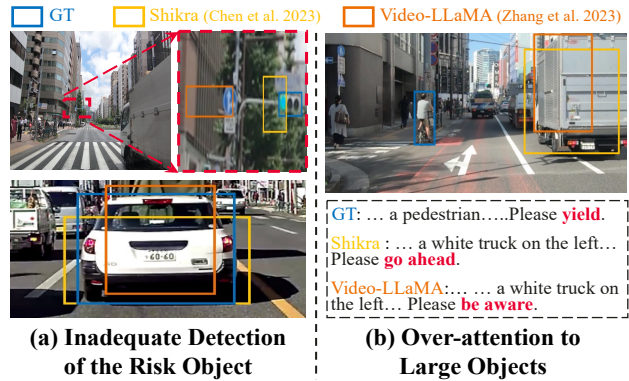


Figure 2: **Illustration of problems of directly adopting MLLM into autonomous driving tasks.** (a) Inadequate Detection for the found risk object. Failure detection of small objects (upper) and inaccurate detection of large objects (below). (b) Over-attention to Large Objects. The MLLMs tend to focus on the large truck instead of the higher-risk pedestrian, leading to the misidentification of the risk object and error suggestions (marked by red).

of MLLMs for autonomous driving.

- We introduce HiLM-D to produce enriched HR feature maps containing vision-specific priors and highlighting high-risk areas, which can seamlessly integrate with and enhance existing MLLMs.
- We conduct experiments on the ROLISP benchmark to demonstrate the superiority of HiLM-D, *e.g.*, outperforming the state-of-the-art MLLMs by 4.8% on BLEU-4 for captioning and 17.2% on mIoU for detection.

Related Work

Multimodal Large Language Models (MLLMs). Natural language processing has witnessed significant strides with the advent of Large Language Models (LLMs) *e.g.*, GPT series (OpenAI 2023; Radford et al. 2019), T5 (Rafel et al. 2020), LLaMA (Touvron et al. 2023) and etc. Motivated by the potential of LLMs, numerous multimodal LLMs (MLLMs), *e.g.*, LLaVA (Liu et al. 2023), MiniGPT-4 (Zhu et al. 2023), Video-LLaMA (Zhang et al. 2023) and InstructBLIP (Dai et al. 2023), have been proposed to expand the LLMs to the multimodal field, *i.e.*, perceiving image/video input, and conversating with users in multiple rounds. Pre-trained on massive image/video-text pairs, the above models can only handle image-level tasks, such as image captioning and question answering. Hence, several works, *e.g.* ContextDET (Zang et al. 2023), KOSMOS-2 (Peng et al. 2023) and Shikra (Chen et al. 2023), have been proposed to enable the grounding ability of MLLMs to produce bounding boxes. However, all of the current MLLMs train the model in low-resolution image-text pairs, presenting limited perception results in high-resolution autonomous driving scenarios; see Fig 2 for examples. In this paper, we propose HiLM-D to enhance the perception ability of current MLLMs for autonomous driving in an efficient way.

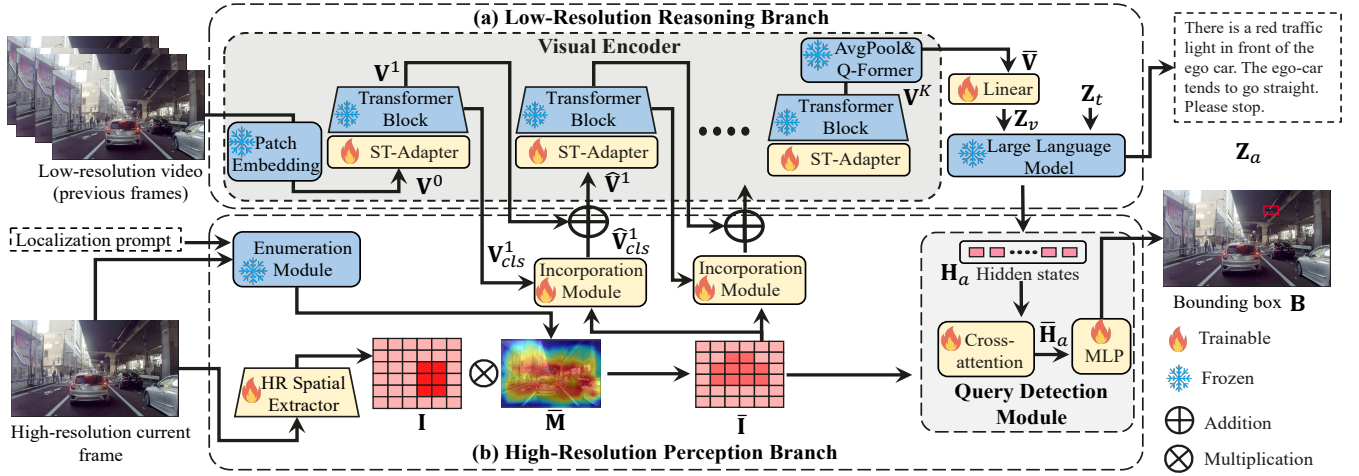


Figure 3: **The overall pipeline of our proposed HiLM-D.** HiLM-D consists of two parts: (a) a low-resolution reasoning branch (LR-RB) to receive the LR video (including current and historical frames) to generate captions about risk objects, reasons, and ego-car actions and (b) a high-resolution perception branch (HR-PB) to input HR current frame to enhance the perception ability of LR-RB in an efficient way.

Multi-tasks in Autonomous Driving. Traditional autonomous driving algorithms individually process different tasks, *e.g.*, detection (Chen et al. 2017), tracking (Petrovskaya and Thrun 2008), reasoning (Kim et al. 2018), and prediction (Ngiam et al. 2021). To extract the richer inter-task information, researchers explore integrating the multi-tasks in the end-to-end training frameworks. For instance, combined training for detection and tracking has been demonstrated in works like D & T (Petrovskaya and Thrun 2008). FaF (Luo, Yang, and Urtasun 2018) takes this further by unifying a detector with a trajectory predictor, yielding notable results. UniAD (Hu et al. 2023) stands out by amalgamating full-stack driving tasks within a singular framework, albeit still relying on distinct sub-networks for each task. A novel direction in this domain is the use of natural language as a unified output across tasks. For instance, ADAPT (Jin et al. 2023) predicts intention and gives explanations using a single caption, while DRAMA (Malla et al. 2023) aims for the risk object detection and explanation. In this paper, we go one step further than Drama and ADAPT, *i.e.*, ROLISP that aims to identify, explain and localize the risk object for the ego-vehicle meanwhile predicting its intention and giving suggestions.

Method

This section details our HiLM-D approach designed to tackle ROLISP using video inputs. As depicted in Fig. 3, our method is end-to-end and consists of two primary components: (a) a low-resolution reasoning branch (LR-RB) to process video semantics to generate captions about risk objects, reasons, and ego-car actions. (b) a high-resolution perception branch (HR-PB) to extract HR feature maps with vision-specific cues from HR images to enhance the perception ability of LR-RB.

Low-Resolution Reasoning Branch

The low-resolution reasoning branch (LR-RB) leverages the MLLM to receive the low-resolution (LR) video input and generates the identified risk object (including reasons) and intentions and suggestions for the ego-vehicle in a natural language manner. As shown in Fig 3 (a), LR-RB comprises a vision encoder and a large language module.

Visual Encoder. The visual encoder transforms video inputs into visual tokens for LLM comprehension. We build the visual encoder based on the pre-trained image vision transformer (ViT) and Q-former, initialized from BLIP2 (Li et al. 2023) and frozen during training. To account for the temporal aspect, which the frozen image ViT overlooks, we incorporate the spatiotemporal adapter (ST-Adapter) (Pan et al. 2022). Formally, given a video with L frames, the ViT maps each frame to its k -th layer feature, resulting in $\mathbf{V}^k = \{\mathbf{v}_i^k\}_{i=1}^L$, where \mathbf{v}_i^k is the feature of i -th frame, $\mathbf{v}_i^k \in \mathbb{R}^{N_v \times D_v}$, N_v is the patch number and D_v is the dimension. This is then processed by the ST-Adapter and a transformer block to produce \mathbf{V}^{k+1} . The ST-Adapter specifics are in the supplementary material. The final video representation, $\bar{\mathbf{V}} \in \mathbb{R}^{N_v \times D_v}$, is derived by applying average pooling and the Q-former to the feature (\mathbf{V}^K) from the ViT’s last layer. A trainable linear layer then projects $\bar{\mathbf{V}}$ to the LLM’s dimension, yielding $\mathbf{Z}_v \in \mathbb{R}^{N_v \times D_l}$.

Large Language Model (LLM). Given the visual tokens, we leverage the pre-trained LLM to produce captions including the risk object with explanations, intentions and suggestions for the ego-car. The input to the LLM is the concatenated multimodal tokens $[\mathbf{Z}_v, \mathbf{Z}_t] \in \mathbb{R}^{(N_v+N_t) \times D_l}$, where $\mathbf{Z}_t \in \mathbb{R}^{N_t \times D_l}$ are the text embeddings, tokenized from text prompts, *e.g.*, ‘Which object is at the highest risk? Then predict the motions and suggestions for the ego-car’. Then, the pre-trained LLM receives the multimodal tokens $[\mathbf{Z}_v, \mathbf{Z}_t]$ to

generate language in an autoregressive way as follows:

$$p(\mathbf{Z}_a | \mathbf{Z}_v, \mathbf{Z}_t) = \prod_{i=1}^L p_\theta(\mathbf{z}_i | \mathbf{Z}_v, \mathbf{Z}_{t,<i}, \mathbf{Z}_{a,<i}), \quad (1)$$

where θ is the trainable parameters, $\mathbf{Z}_a \in \mathbb{R}^{N_a \times D_t}$ is the generated answer, $\mathbf{Z}_{t,<i}$ and $\mathbf{Z}_{a,<i}$ are the prompts and answer tokens before the current prediction token \mathbf{z}_i . The ST-Adapters and the linear layer are supervised by the caption loss $\mathcal{L}_{cap} = CE(\mathbf{Z}_a, \hat{\mathbf{Z}}_a)$, where $\hat{\mathbf{Z}}_a$ is the ground-truth answer, CE is the cross-entropy loss.

High-Resolution Perception Branch

The high-resolution perception branch (HR-PB) is tailored to integrate vision-specific information from the high-resolution images and features associated with potential high-risk objects into LR-RB. As shown in Fig. 3 (b), the proposed branch consists of four parts: an HR spatial extractor (HRSE) to obtain HR features for the HR frame; an enumeration module to underscore all potential high-risk objects; an incorporation module to integrate the all potential risk objects into LR-RB; a query detection head to detect objects based on the HR features.

HR spatial extractor (HRSE). To capture vision-specific information for object detection, the HRSE is modified from the classic convolution network (CNN) ResNet (He et al. 2016) (see the supplementary material). Compared with the plain ViT in current MLLMs, CNN incurs many advantages: reducing the memory and computation resources, and bringing vision-specific prior for the detection tasks (e.g., local connectivity and spatial invariance). We prove this in Table 4. We denote the extracted HR spatial feature map as $\mathbf{I} \in \mathbb{R}^{H \times W \times D_i}$, where D_i , H and W are the dimension, width and height respectively.

Enumeration module. In autonomous driving, some risk objects, i.e., persons or traffic cones, may only occupy a small part of the entire image, and usually at the edge area. However, our experiments revealed that existing MLLMs tend to prioritize more prominent objects, like large vehicles, leading to misidentification of the risk object. To address this, we introduce an enumeration module, ensuring the model pays attention to all potential high-risk object regions rather than just the dominant ones. This module utilizes pre-trained MLLMs to measure the similarity between the image and localization prompts, such as ‘Where are the vehicles, traffic lights/cones, and people?’. Subsequently, GradCAM (Selvaraju et al. 2017) is employed to produce a map that emphasizes these high-risk object areas. Further specifics are available in the supplementary material. We denote the generated highlight map as $\mathbf{M} \in \mathbb{R}^{H_m \times W_m \times 1}$, where H_m and W_m are the width and height of the highlight map, and the value is at the range from 0 to 1. Then, we up-sample \mathbf{M} to the size equal to \mathbf{I} , yielding $\bar{\mathbf{M}} \in \mathbb{R}^{H \times W \times 1}$. Finally, we obtain the highlighted HR image feature $\bar{\mathbf{I}} = \bar{\mathbf{M}} \cdot \mathbf{I}$, where \cdot is the element-wise multiplication and $\bar{\mathbf{I}} \in \mathbb{R}^{H \times W \times D_i}$.

Incorporation module. The incorporation module aims to let semantics learned from LR-RB assimilate the spatial fea-

tures with all potential risk objects, thus allowing the LLM to compare and decide which one needs the most attention. We achieve this by a cross-attention module that regards the features from the k -th layer of LR-RB (\mathbf{V}^k) as the query, the highlighted HR feature maps $\bar{\mathbf{I}}$ as the value and key. For efficient computation, we only use the cls token from $\mathbf{V}^k = [\mathbf{V}_{cls}^k, \mathbf{V}_{patch}^k]$ as the query, i.e., \mathbf{V}_{cls}^k . Then, the cross-attention can be formulated as $\bar{\mathbf{V}}_{cls}^k = CA(\mathbf{V}_{cls}^k, \bar{\mathbf{I}})$. After adding $\bar{\mathbf{V}}_{cls}^k \in \mathbb{R}^{L \times D_v}$ to the original \mathbf{V}_{cls}^k , we obtain the new cls token, i.e., $\hat{\mathbf{V}}_{cls}^k = \alpha \bar{\mathbf{V}}_{cls}^k + \mathbf{V}_{cls}^k$, for the $i + 1$ -th ST-Adapter and transformer block. α is a learnable gating factor to adaptively control the importance of $\bar{\mathbf{V}}_{cls}^k$, which is initialized by zero to avoid bringing disturbance to the original ViT during the beginning of the training. Finally, the incorporated vision tokens is acquired by $\hat{\mathbf{V}}^k = [\hat{\mathbf{V}}_{cls}^k, \mathbf{V}_{patch}^k]$.

Query detection head. For obtaining precise bounding boxes, we devise a query detection head to regard the representation of found risk object as the prior knowledge to find the bounding box in the HR features i.e., \mathbf{I} . To achieve this, we use the hidden states of the risk object as the query, the highlighted HR spatial feature as the value and key to compute the cross-attention, which can be formulated as $\bar{\mathbf{H}}_a = CA(\mathbf{H}_a, \bar{\mathbf{I}})$, where $\mathbf{H}_a \in \mathbb{R}^{N_a \times D_h}$ is the hidden states of languages tokens related to the answer, i.e., the found object. Finally, $\bar{\mathbf{H}}_a$ is fed to the MLP to generate the bounding box, i.e., $\mathbf{B} = MLP(\bar{\mathbf{H}}_a) \in \mathbb{R}^{N \times 4}$. Then, the predicted box is supervised by $\mathcal{L}_{box} = L1(\mathbf{B}, \hat{\mathbf{B}})$, where $L1$ is the L1 loss and $\hat{\mathbf{B}}$ is the ground-truth box.

The overall loss is defined as follows:

$$\mathcal{L} = \mathcal{L}_{cap} + \lambda_{box} \mathcal{L}_{box}, \quad (2)$$

where λ_{box} is the hyper-parameters.

Experiments

Experimental Settings

Implementation details. Our proposed method is implemented in PyTorch (Paszke et al. 2019) trained using a single machine with 8 NVIDIA V100 GPUs. The input video frames are resized and cropped to the spatial size of 224×224 . We uniformly sample $L = 5$ frames from the entire video, and ensure that the last frame is sampled for producing bounding boxes. We set λ_{box} in Eq. 2 to 2. We use AdamW (Loshchilov and Hutter 2017) as the optimizer and cosine annealing scheduler (Loshchilov and Hutter 2016) as the learning rate scheduler with an initial learning rate of $1e-4$ for the low-resolution reasoning branch and $4e-4$ for the high-resolution perception branch, and global batch size of 64.

Datasets. DRAMA (Malla et al. 2023) is a benchmark evaluating visual reasoning in driving scenarios with 17,785 two-second interactive scenarios. However, it only provides captions about risk objects without intentions or suggestions for the ego-vehicle, essential for ROLISP. To address this, we enhance the annotations, extending the DRAMA captions to include ego-vehicle intentions and suggestions, re-

Table 1: **Comparison with the state-of-the-art.** For all metrics, the higher the scores, the better the results. ‘Ours w/o ST’ means our model without ST-Adapters. ‘B4’, ‘M’, ‘C’ and ‘S’ refer to BLEU-4, METEOR, CIDER and SPICE. ‘AVG’ is the average value of B4 and mIoU. All results are obtained by fine-tuning the models on DRAMA-ROLISP in the same setting. The entries noted in grey are the results of our method. * indicates that the model is pre-trained on large object detection datasets.

Input	Method	Captioning				Detection				AVG
		B4	M	C	S	mIoU	IoU _S	IoU _M	IoU _L	
Image	BLIP-2	46.1	34.3	194.7	50.7	46.3	8.1	60.2	73.7	46.2
	LLaVA	47.5	35.2	198.6	48.3	47.2	8.0	62.1	74.2	47.4
	InstructBLIP	49.9	37.9	205.0	50.9	47.8	9.1	62.2	74.5	48.9
	Shikra*	49.8	37.7	204.7	50.7	50.3	10.4	59.5	73.8	50.1
	Ours w/o ST	55.8	39.1	237.5	53.4	59.6	31.2	62.3	82.9	57.7
Video	eP-ALM	51.4	38.0	225.1	52.8	43.2	7.2	56.8	68.8	47.3
	Video-LLaMA	53.9	37.8	229.5	52.6	42.8	6.9	55.3	67.9	48.4
	Ours	58.5	41.2	279.2	57.8	59.2	31.1	62.5	82.3	58.9

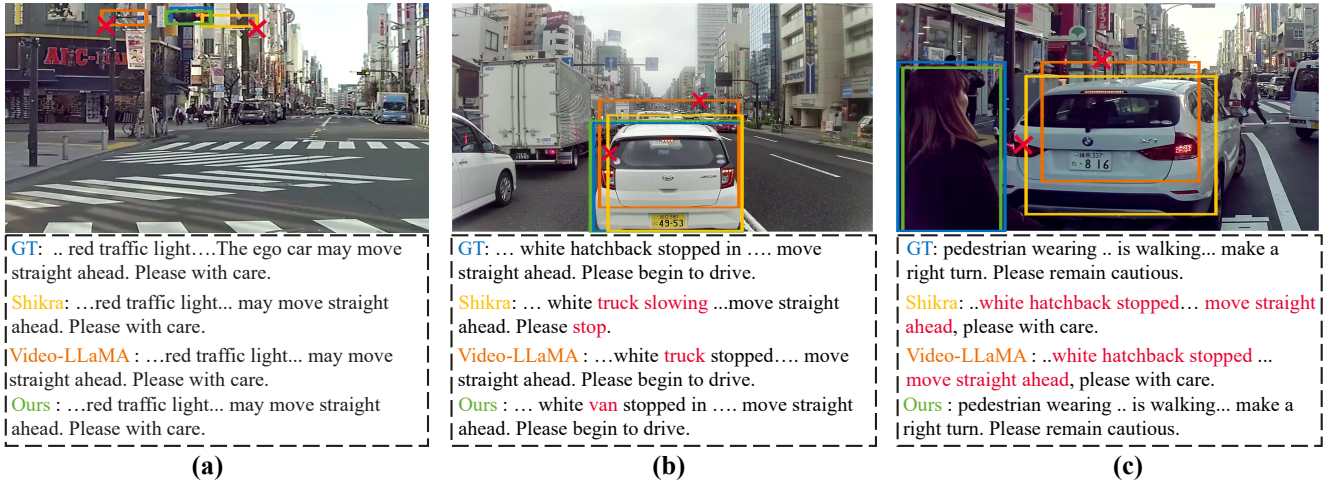


Figure 4: **The visualization comparison with the the state-of-the-art.** For clarity, we only show some keywords of the full captions. The inaccurate bounding box and error-predicted words in captions are marked by red. Compared with the current MLLMs, Our model can (a) detect the small object, *i.e.*, traffic light, (b) generate more precise bounding boxes and (c) accurately identify the highest risk object.

sulting in the DRAMA-ROLISP dataset. Further dataset details are in the supplementary material.

Evaluation metrics. ROLISP comprises two tasks: (1) captioning to identify and explain risk objects while predicting ego-vehicle intentions and motions, and (2) risk object detection. Captioning performance follows standard metrics (Malla et al. 2023), *i.e.*, BLEU-4 (B4), METEOR (M), CIDER (C), and SPICE (S). We employ the mean intersection over union (mIoU) for detection assessment. Additionally, we present IoU scores categorized by object size: small (IoU_S), medium (IoU_M), and large (IoU_L).

Comparison with the State-of-the-Art Methods

We conduct the experiments on DRAMA-ROLISP to compare with both image-based and video-based MLLMs, including BLIP-2 (Li et al. 2023), LLaVA (Liu et al. 2023), InstructBLIP (Dai et al. 2023), Shikra (Chen et al. 2023), eP-ALM (Shukor, Dancette, and Cord 2023), and Video-LLaMA (Zhang et al. 2023); Note that except for Shikra, other models have no ability to detect objects. Hence, we integrate the detection head (MLP based) into them for bound-

ing boxes; see details in the supplementary material.

Table 1 demonstrates the superior performance of our method in both captioning and detection tasks. Video-based approaches generally surpass image-based ones in captioning, benefiting from temporal data for enhanced risk identification and intention/suggestion prediction. However, their detection capabilities tend to decline, possibly due to the redundant noise in videos affecting object detection. Uniquely, our video-based approach enhances captioning performance (*e.g.*, B4 score increases from 55.8 to 58.5) without compromising detection accuracy. Notably, we observe significant improvements for small objects, underscoring the advantages of high-resolution input. Fig.4 offers a visual comparison of captioning and detection results from Shikra(Chen et al. 2023), Video-LLaMA (Zhang et al. 2023), and our method, further highlighting our superior performance in both domains.

Ablation Study

In this section, we conduct the ablation study to evaluate and analyze the high-resolution perception branch (HR-PB)

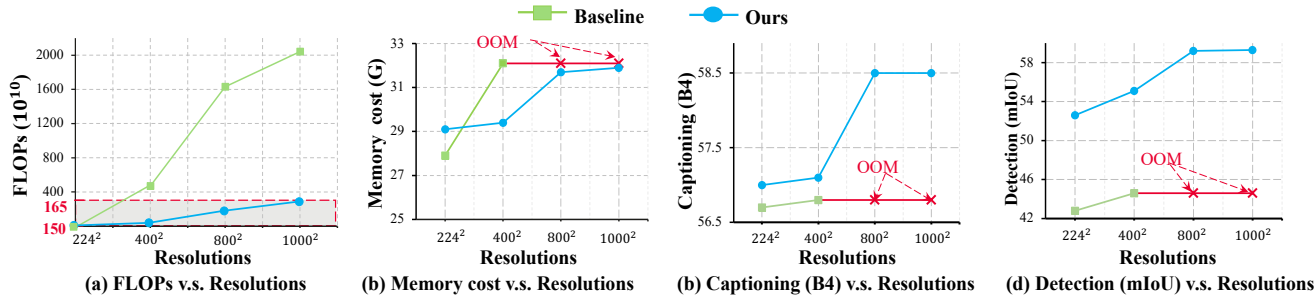


Figure 5: **Comparison of the baseline and ours across different resolution inputs.** The baseline processes varying resolution videos, while our method, thanks to HR-PB, uses a single high-resolution image. "OOM" indicates out of memory. FLOPs and memory metrics are based on a V100 GPU with a batch size of one, and FLOPs values are scaled to 10^{10} for clarity. (a) FLOPs v.s. Resolutions. (b) Memory cost v.s. Resolutions. (c) Captioning (B4) v.s. Resolutions. (d) Detection (mIoU) v.s. Resolutions.

Table 2: **Ablation study of modules in HR-PB.** 'HRES', 'EM', 'IM' and 'QDH' mean the HR spatial extractor, the enumeration module, the incorporation module, and the query detection head respectively. 'w/o' indicates our model without the specific module.

	Model	Captioning B4	Detection mIoU	AVG
(a)	Ours	55.8	59.6	57.7
(b)	Ours w/o HRES	55.9	42.4 (-17.2)	49.2
(c)	Ours w/o QDH	55.8	46.7 (-12.9)	51.3
(d)	Ours w/o IM	52.8 (-3.0)	53.5 (-6.1)	53.2
(e)	Ours w/o EM	54.1 (-1.7)	56.4 (-3.2)	55.3
(f)	Baseline (LR-RB)	51.8 (-4.0)	40.5 (-19.1)	46.2

(Fig. 3 (b)), the key part of the proposed HiLM-D. Unless otherwise specified, the baseline model is the low-resolution reasoning branch (Fig. 3 (a)) excluding the ST-Adapter to reduce training overhead; see more details in the supplementary material.

The effect of each module in HR-PB. Table 2 reports the effect of our proposed modules in HR-PB. From the table, we have the following observations: (i) Compared with the line *a* and *f*, we find that the improvements mainly come from our proposed HR-RB. (ii) Compared with the line (a)-(c), HRES and QDH are essential for the detection performance, e.g., without HRES and QDH dropping 17.2% and 12.9% respectively in terms of the mIoU score. (iii) Compared with the line (a), (d) and (e), IM and EM benefit both caption and detection performance. Specifically, the model without IM would degrade 3.0% and 6.1% in terms of B4 and mIoU, since the captured highlighted can not be integrated into the MLLM. Moreover, without EM, the model would tend to focus on the salient objects, thus having conclusive defects, e.g., dropping 1.7% and 3.2% on the caption and detection performance.

We also show the visualization of the caption and detection results of each model in Fig. 6. Without HRES and QDH, the models show poor detection results, e.g., (b) produces a bounding box containing non-object while (c) generates an inaccurate box for the pedestrian. Additionally, the model without IM and EM, i.e., (d) and (e), would tend to predict the large objects (the white truck) while missing the

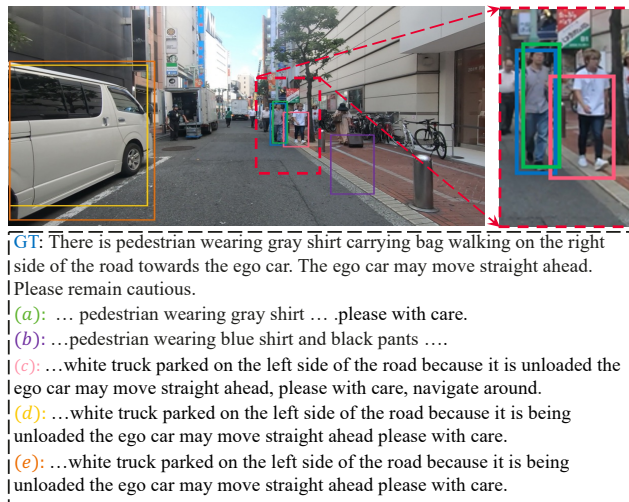


Figure 6: **The visualization of caption and detection results.** (a)-(e) are the models presented in Table 2. We display the complete GT caption but for predictions from models (a)-(e), only differing words from GT are shown.

actual risk object (pedestrian wearing blue shirt and black pants). The full model, i.e., (a), combined with all modules achieve promising results.

Performance comparison of the baseline and ours across different resolution inputs. An intuitive way to enhance the perception ability is to increase the resolution of inputs. To further study the effectiveness of our proposed HR-PB, we conduct experiments to compare the baseline and our method across different resolution inputs in Fig. 5. Specifically, inputs of varying resolutions are fed into the baseline and our method respectively. Note that the baseline model in this ablation is the model with ST-Adapter, hence can receive HR videos, while ours only feed one current HR frame. From Fig. 5, we can see that as the input video resolution increases, the FLOPs of the baseline model grow proportionally. For example, as the input resolution escalates from 224^2 to 1000^2 , the FLOPs of the baseline increase from 156.9 to 2040.2, a 13 times growth. Differently, benefiting from HR-PB, our approach requires only a single

Table 3: **The versatility of HR-PB.** We evaluate both image and video-based methods, specifically BLIP-2 and Video-LLaMA, under consistent settings.

Model	Captioning B4	Detection mIoU	AVG
BLIP-2	46.1	46.3	46.2
+ HR-PB	50.6 (+4.5)	59.1 (+12.8)	54.9 (+8.7)
Video-LLaMA	53.9	42.8	48.4
+ HR-PB	56.7 (+2.8)	58.9 (+16.1)	57.8 (+9.4)

Table 4: **Ablation study on the choice of HR spatial extractor.** We choose four advanced models where two contain vision-specific prior, *i.e.*, ResNet50 and ResNet101 and others without the prior, *i.e.*, ViT-B and ViT-L. ‘Pre-train’ indicates that we use the weight pre-trained on ImageNet. Note that FLOPs and memory cost is computed for the whole model.

Model	Pre-train	Memory ↓	FLOPs ↓	mIoU ↑
ResNet50	✗	27.8G	158.3	54.0
ResNet50	✓			55.1
ResNet101	✗	28.2G	159.5	54.5
ResNet101	✓			55.9
ViT-B	✗	29.8G	162.2	44.7
ViT-B	✓			48.9
ViT-L	✗	31.3G	174.5	45.8
ViT-L	✓			49.1

high-resolution image, significantly reducing FLOPs, only increasing 1.05 times. Furthermore, the baseline model encounters OOM issues when the resolution exceeds 400². In contrast, our approach remains stable up to a resolution of 1000². In summary, our method can outperform the baseline model while using much less computation and memory cost.

The versatility of HR-PB. Table 3 demonstrates that our proposed HR-PB can be applied to existing MLLMs to improve their performance on ROLISP. Specifically, with our HR-PB, BLIP-2 (Li et al. 2023) sees improvements of 4.5% in B4 and 13.8% in mIoU scores, while Video-LLaMA (Zhang et al. 2023) benefits with gains of 2.8% and 16.1% in captioning and detection results, respectively.

Effect of Different Designs

Here, we conduct the experiment to analyse the effect of different designs, *i.e.*, the choice of the HR spatial extractor, the number of the incorporation module and the types of the query detection head.

The choice of the backbone of HR spatial extractor (HRSE). In Table 4, we conduct experiments to analyze the effect of different backbones of HRSE. For saving resources, we use the resolution of 400² to train all models in the same setting. From the table, we can find that (1) the plain ViT without the vision-specific prior achieves limited performance on detection. (2) using the advanced backbones would benefit the detection performance while bringing more memory and computation cost; (3) pre-trained weight would improve the performance. Since the performance gain obtained by the advanced backbones is limited,

Table 5: **Ablation study of the number of the incorporation module.** The model performs best when the number is set to 3.

Number	Captioning B4	Detection mIoU	AVG
1	55.1	52.2	53.7
2	55.4	56.8	56.1
3	55.8	59.6	57.7
4	55.8	59.4	57.6

Table 6: **Ablation study of the types of the query head detection.** ‘LLM’ indicates directly using LLM to regress the position *i.e.*, bounding boxes, using numerical values in natural language similar to Shikra (Chen et al. 2023). ‘DETR’ means the modified decoder used in DETR (Carion et al. 2020).

Type	Captioning B4	Detection mIoU	AVG
LLM	55.8	48.9	52.4
DETR	55.8	56.3	56.1
Ours	55.8	59.6	57.7

we use ResNet50 as the backbone for efficiency.

The numbers of the incorporation module (IM). In Table 5, we study the effect of numbers of IM. We uniformly incorporate IM into the ViT of LR-RB. We find that the model accuracy saturates when the numbers go larger. For example, as the number arises from 1 to 3, the mIoU achieves 7.4% improvement. We also find that adding more IM cannot monotonically promote performance when the number is larger than 3. Therefore, we empirically set the number to 3 by default.

Types of the query detection head (QDH). Table 6 shows the experiments to analyze the effect of the different types of QDH. Besides ours shown in Fig. 3 (b), we select two other modules to compare, *i.e.*, directly using LLM to regress the bounding boxes using numerical values as Shikra (Chen et al. 2023) and the modified decoder in DETR (Carion et al. 2020). The results show that using LLM achieves limited performance in detection, which shows that our method is more effective in this small-scale detection dataset. Moreover, ours performs better than DETR, *e.g.*, 59.6% vs 56.3% on the detection task due to prior knowledge.

Conclusion

We introduce a novel approach using multimodal large language models (MLLMs) to unify multiple driving tasks, termed Risk Object Localization and Intention and Suggestion Prediction (ROLISP). We further propose HiLM-D to produce enriched HR feature maps containing vision-specific priors and highlighting high-risk areas, which can seamlessly integrate with and enhance existing MLLMs. Our extensive evaluations prove the superiority of HiLM-D. **Limitations.** It is worth noting the inherent limitations of our dataset. Specifically, each video contains only one risk object, which might not capture the complexity of real-world scenarios. Additionally, the dataset lacks extreme weather conditions like rain or fog, which are crucial for compre-

hensive autonomous driving evaluations. Furthermore, the suggestions provided are typically concise, such as 'stop' or 'yield', potentially oversimplifying the range of possible actions. Our future work is to curate a more diverse and challenging dataset, advancing the field further.

References

- Caesar, H.; Bankiti, V.; Lang, A. H.; Vora, S.; Liong, V. E.; Xu, Q.; Krishnan, A.; Pan, Y.; Baldan, G.; and Beijbom, O. 2020. nuscenes: A multimodal dataset for autonomous driving. In *Proceedings of the IEEE/CVF conference on computer vision and pattern recognition*, 11621–11631.
- Carion, N.; Massa, F.; Synnaeve, G.; Usunier, N.; Kirillov, A.; and Zagoruyko, S. 2020. End-to-end object detection with transformers. In *European conference on computer vision*, 213–229. Springer.
- Chen, K.; Zhang, Z.; Zeng, W.; Zhang, R.; Zhu, F.; and Zhao, R. 2023. Shikra: Unleashing Multimodal LLM's Referential Dialogue Magic. *arXiv preprint arXiv:2306.15195*.
- Chen, X.; Ma, H.; Wan, J.; Li, B.; and Xia, T. 2017. Multi-view 3d object detection network for autonomous driving. In *Proceedings of the IEEE conference on Computer Vision and Pattern Recognition*, 1907–1915.
- Chen, Z.; Duan, Y.; Wang, W.; He, J.; Lu, T.; Dai, J.; and Qiao, Y. 2022. Vision Transformer Adapter for Dense Predictions.
- Dai, W.; Li, J.; Li, D.; Huat, A.; Zhao, J.; Wang, W.; Li, B.; Fung, P.; and Hoi, S. 2023. InstructBLIP: Towards General-purpose Vision-Language Models with Instruction Tuning.
- Dosovitskiy, A.; Beyer, L.; Kolesnikov, A.; Weissenborn, D.; Zhai, X.; Unterthiner, T.; Dehghani, M.; Minderer, M.; Heigold, G.; Gelly, S.; et al. 2020. An image is worth 16x16 words: Transformers for image recognition at scale. *arXiv preprint arXiv:2010.11929*.
- He, K.; Zhang, X.; Ren, S.; and Sun, J. 2016. Deep Residual Learning for Image Recognition. In *2016 IEEE Conference on Computer Vision and Pattern Recognition (CVPR)*.
- Hu, Y.; Yang, J.; Chen, L.; Li, K.; Sima, C.; Zhu, X.; Chai, S.; Du, S.; Lin, T.; Wang, W.; et al. 2023. Planning-oriented autonomous driving. In *Proceedings of the IEEE/CVF Conference on Computer Vision and Pattern Recognition*, 17853–17862.
- Jin, B.; Liu, X.; Zheng, Y.; Li, P.; Zhao, H.; Zhang, T.; Zheng, Y.; Zhou, G.; and Liu, J. 2023. Adapt: Action-aware driving caption transformer. *arXiv preprint arXiv:2302.00673*.
- Kim, J.; Rohrbach, A.; Darrell, T.; Canny, J.; and Akata, Z. 2018. Textual explanations for self-driving vehicles. In *Proceedings of the European conference on computer vision (ECCV)*, 563–578.
- Li, J.; Li, D.; Savarese, S.; and Hoi, S. 2023. Blip-2: Bootstrapping language-image pre-training with frozen image encoders and large language models. *arXiv preprint arXiv:2301.12597*.
- Liu, H.; Li, C.; Wu, Q.; and Lee, Y. J. 2023. Visual instruction tuning. *arXiv preprint arXiv:2304.08485*.
- Liu, Z.; Lin, Y.; Cao, Y.; Hu, H.; Wei, Y.; Zhang, Z.; Lin, S.; and Guo, B. 2021. Swin transformer: Hierarchical vision transformer using shifted windows. In *Proceedings of the IEEE/CVF international conference on computer vision*, 10012–10022.
- Loshchilov, I.; and Hutter, F. 2016. Sgdr: Stochastic gradient descent with warm restarts. *arXiv preprint arXiv:1608.03983*.
- Loshchilov, I.; and Hutter, F. 2017. Decoupled weight decay regularization. *arXiv preprint arXiv:1711.05101*.
- Luo, W.; Yang, B.; and Urtasun, R. 2018. Fast and furious: Real time end-to-end 3d detection, tracking and motion forecasting with a single convolutional net. In *Proceedings of the IEEE conference on Computer Vision and Pattern Recognition*, 3569–3577.
- Malla, S.; Choi, C.; Dwivedi, I.; Choi, J. H.; and Li, J. 2023. DRAMA: Joint Risk Localization and Captioning in Driving. In *Proceedings of the IEEE/CVF Winter Conference on Applications of Computer Vision*, 1043–1052.
- Ngiam, J.; Caine, B.; Vasudevan, V.; Zhang, Z.; Chiang, H.-T. L.; Ling, J.; Roelofs, R.; Bewley, A.; Liu, C.; Venugopal, A.; et al. 2021. Scene transformer: A unified multi-task model for behavior prediction and planning. *arXiv preprint arXiv:2106.08417*, 2(7).
- OpenAI, O. 2023. GPT-4 Technical Report.
- Pan, J.; Lin, Z.; Zhu, X.; Shao, J.; and ST-Adapter, H. L. 2022. Parameter-efficient image-to-video transfer learning for action recognition. *Preprint at https://arxiv.org/abs/2206.13559*.
- Paszke, A.; Gross, S.; Massa, F.; Lerer, A.; Bradbury, J.; Chanan, G.; Killeen, T.; Lin, Z.; Gimelshein, N.; Antiga, L.; et al. 2019. Pytorch: An imperative style, high-performance deep learning library. *Advances in neural information processing systems*, 32.
- Peng, Z.; Wang, W.; Dong, L.; Hao, Y.; Huang, S.; Ma, S.; and Wei, F. 2023. Kosmos-2: Grounding Multimodal Large Language Models to the World. *arXiv preprint arXiv:2306.14824*.
- Petrovskaya, A.; and Thrun, S. 2008. Model based vehicle tracking for autonomous driving in urban environments. *Proceedings of robotics: science and systems IV, Zurich, Switzerland*, 34.
- Radford, A.; Wu, J.; Child, R.; Luan, D.; Amodei, D.; Sutskever, I.; et al. 2019. Language models are unsupervised multitask learners. *OpenAI blog*, 1(8): 9.
- Raffel, C.; Shazeer, N.; Roberts, A.; Lee, K.; Narang, S.; Matena, M.; Zhou, Y.; Li, W.; and Liu, P. J. 2020. Exploring the limits of transfer learning with a unified text-to-text transformer. *The Journal of Machine Learning Research*, 21(1): 5485–5551.
- Selvaraju, R. R.; Cogswell, M.; Das, A.; Vedantam, R.; Parikh, D.; and Batra, D. 2017. Grad-CAM: Visual Explanations from Deep Networks via Gradient-based Localization. In *2017 IEEE International Conference on Computer Vision (ICCV)*.

Shukor, M.; Dancette, C.; and Cord, M. 2023. eP-ALM: Efficient Perceptual Augmentation of Language Models. *arXiv preprint arXiv:2303.11403*.

Sun, P.; Kretzschmar, H.; Dotiwalla, X.; Chouard, A.; Patnaik, V.; Tsui, P.; Guo, J.; Zhou, Y.; Chai, Y.; Caine, B.; et al. 2020. Scalability in perception for autonomous driving: Waymo open dataset. In *Proceedings of the IEEE/CVF conference on computer vision and pattern recognition*, 2446–2454.

Touvron, H.; Lavril, T.; Izacard, G.; Martinet, X.; Lachaux, M.-A.; Lacroix, T.; Rozière, B.; Goyal, N.; Hambro, E.; Azhar, F.; et al. 2023. Llama: Open and efficient foundation language models. *arXiv preprint arXiv:2302.13971*.

Wang, W.; Chen, Z.; Chen, X.; Wu, J.; Zhu, X.; Zeng, G.; Luo, P.; Lu, T.; Zhou, J.; Qiao, Y.; et al. 2023. Visionllm: Large language model is also an open-ended decoder for vision-centric tasks. *arXiv preprint arXiv:2305.11175*.

Wang, W.; Xie, E.; Li, X.; Fan, D.-P.; Song, K.; Liang, D.; Lu, T.; Luo, P.; and Shao, L. 2022. Pvt v2: Improved baselines with pyramid vision transformer. *Computational Visual Media*, 8(3): 415–424.

Zang, Y.; Li, W.; Han, J.; Zhou, K.; and Loy, C. C. 2023. Contextual Object Detection with Multimodal Large Language Models. *arXiv preprint arXiv:2305.18279*.

Zhang, H.; Li, X.; Bing, L.; and at al. 2023. Video-llama: An instruction-tuned audio-visual language model for video understanding. *arXiv preprint arXiv:2306.02858*.

Zhu, D.; Chen, J.; Shen, X.; Li, X.; and Elhoseiny, M. 2023. Minigt-4: Enhancing vision-language understanding with advanced large language models. *arXiv preprint arXiv:2304.10592*.